ELSEVIER

Chemical Engineering Journal 137 (2008) 428–435

Chemical Engineering Journal

www.elsevier.com/locate/cej

Fabrication of hierarchical ZnO films with interwoven porous conformations by a bioinspired templating technique

Qun Dong [a], Huilan Su [a,*], Chunfu Zhang [b], Di Zhang [a], Qixin Guo [c], Fabian Kiessling [d]

[a] *State Key Lab of Metal Matrix Composites, Shanghai Jiaotong University, Shanghai 200030, PR China*
[b] *Shanghai Institute of Applied Physics, Chinese Academy of Sciences, Shanghai 201800, PR China*
[c] *Department of Electrical and Electronic Engineering, Saga University, Saga 840-8502, Japan*
[d] *Junior Group Molecular Imaging, Department of Medical Physics in Radiology, German Cancer Research Center, Heidelberg 69120, Germany*

Received 28 February 2007; received in revised form 19 May 2007; accepted 21 May 2007

Abstract

Hierarchical biomorphic ZnO films are prepared by a simple soakage procedure associated with succedent calcination treatment, using natural eggshell membrane (ESM) as the template. The hierarchy of ESM architecture is faithfully achieved by the assembly of ZnO nanocrystallites into interwoven meshwork at three dimensions. The thermal evolution, phase, morphology and pore size distribution of the samples are characterized by thermogravimetric analysis (TGA), X-ray diffraction (XRD), transmission electron microscopy (TEM), Fourier transform infrared (FTIR) spectroscopy, field emission gun scanning electron microscopy (FESEM) and nitrogen isothermal adsorption measurement. Based on the detailed investigation, a possible synthesis mechanism is discussed here.

Keywords: ZnO nanostructures; Biocrystallization; Controlled growth; Porous thin solid films

1. Introduction

As a wide band gap semiconductor with a large excitation binding energy (60 meV), zinc oxide becomes one of the most important functional materials with unique properties of near-UV emission, optical transparency, electric conductivity, and piezoelectricity [1]. Especially, the good performance for field emission makes hierarchical ZnO nanostructures promising candidates for microelectronic devices [2]. In recent years, ultraviolet lasing from ZnO nanostructure has been demonstrated to trigger a wide range of subsequent research on ameliorative synthesis [3–8]. However, conventional approaches are complicated and difficult to construct practical and functional ZnO with hierarchical nanostructures.

Nowadays mimicking the biomineralization process integrating templating synthesis and self-organization, has become an important tool for exquisite fabrication of sophisticated architectures. Nature always fascinates scientists and engineers, lying on numerous examples of wonderful biostructures with optimized shapes and patterns. Enlightened by the bioinspiration, scientists have utilized quite a list of biological species including DNA and viruses, skeletal plates, butterfly wings, shell membranes, silk fibers, papers and plant [9–15] to synthesize hierarchical functional materials with sophisticated structure and ordering [16,17]. In addition, compared with many man-made top-down materials, some bottom-up nanomaterials assembled from nanoscopic to macroscopic scale show relevant unique properties. Therefore, it is essential to exploit valuable bioinspired techniques for constructing self-assembled nanostructures sufficing special superior functionality.

There are some inherent limitations in various methods for nanostructured materials. As for the CVD route, it is feasible only for those precursors with high volatility and thermal stability, which limited its applications in many cases. Since pioneered by Davis et al. [18] in synthesizing macrostructured silica and zeolite from bacterial thread templates, most research on the replication of biological organizations has adopted the sol–gel route. It is based on the adsorption of metal-alkoxide molecules from solution onto hydroxylated surfaces and a subsequent hydrolysis to give metal oxide/organic nanocomposite films with molecular precision [19]. Moreover, wet-chemical

* Corresponding author. Tel.: +86 21 62933106; fax: +86 21 62822012.
E-mail address: hlsu@sjtu.edu.cn (H. Su).

1385-8947/$ – see front matter © 2007 Elsevier B.V. All rights reserved.
doi:10.1016/j.cej.2007.05.045

techniques have succeeded in biomorphic synthesis of a group of structures such as ropes, helixes, spirals, gyroids, doughnuts, and discoids, and even hierarchically ordered crystals [17–24], relating to a wide range of metallic [25,26], semiconductor [27,28], and oxide nanocrystals [29]. Consequently, the bioinspired synthesis associated with wet-chemical technique should be a perfect approach to fabricate those nanomaterials with predetermined structures and relevant unique properties.

Herein, we report a novel bioinspired route to assemble hierarchical ZnO films with interwoven mesoporous conformations. Considering the special protein patterns and relevant functional groups of eggshell membrane (ESM) ingredients, we choose the convenient biomaterial ESM as the biotemplate to fabricate hierarchical ZnO fibrous networks through a solution soakage approach followed by a thermal treatment. Based on the formation and assembly of ZnO nanocrystallites, as-prepared hierarchical ZnO films faithfully reproduce the morphology and the hierarchy of natural ESM from nanometer to macroscopic scale. This bioinspired method provides a simple and green route to fabricate advanced crystalline materials at intricate but well-organized modes.

2. Experimental

2.1. Sample preparation

Eggshell membrane was separated from the $CaCO_3$ shell of commercial eggs and washed with distilled water. ESM pieces were cut into quadrilateral sheets of about 1 cm in side length and dried at room temperature in airflow. Subsequently, the above ESM sheets were immersed into 0.5 M $Zn(NO_3)_2$ ethanol solution (pH 2–5) for 13 h at room temperature. After being fished out and rinsed with distilled water, the templated hybrids were dried naturally and calcined at different temperatures (450, 550, and 700 °C) for 1.5 h to remove organic ESM and achieve better crystallization of the sinters. The resulting white sheets were stored in vacuum for further characterizations. Thermogravimetric analysis (TGA, TA Instruments Inc., TGA2050) was conducted on the impregnated ESM (the hybrids) compared with that of the original as-prepared ESM sheets. It revealed that the hybrids started to be pyrolysed at 200 °C and left 17.9% (by mass) inorganic sinters at 550 °C while the original ESM also started to be pyrolysed at 200 °C and were completely decomposed at 550 °C.

2.2. Characterization

X-ray diffraction (XRD) measurements were carried out on a Rigaku D/max 2550 V instrument with Cu Kα radiation (λ = 1.5406 Å). The morphologies were investigated on a FEI Sirion 200 field emission gun scanning electron microscope (FESEM). Transmission electron microscopy (TEM) and high-resolution transmission electron microscopy (HRTEM) images were conducted on a JEOL JEM-2010 instrument and a JEOL JEM-2100F instrument, respectively, and examined by selected area electron diffraction (SAED). Fourier-transform infrared (FTIR) spectra of the samples were recorded on a Bruker EQUINOX55 instrument at a resolution of 0.5 cm^{-1} and a spectral range 400–4000 cm^{-1}. All spectra were recorded at room temperature in air. The adsorption and desorption isotherm studies with liquid nitrogen were performed using a Micromeritics ASAP 2010 M + C system. The specific surface area (SSA) was examined using a single point Brunauer–Emmett–Teller (BET) method. The pore-size distribution was calculated from the adsorption branch of the nitrogen isotherm, using the Barrett–Joyner–Halenda method.

3. Results and discussion

Fig. 1 shows the XRD patterns of the sinters prepared at various temperatures as well as the templated hybrids (as-impregnated eggshell membrane kept into 0.5 M $Zn(NO_3)_2$ ethanol solution at pH 2 for 13 h). The hybrids, containing zinc precursors and organic bioingredients, are mainly amorphous. After calcined at 450 °C, there is partial crystallization of hexagonal ZnO with a zincite structure (SG: *P*63*mc*, JCPDS 36-1451). Based on the TGA results, it can be concluded that the biotemplate ESM is not thoroughly decomposed at this temperature. It also presents additional peaks pointing to the presence of the amorphous charring products. The well-established crystallization process is achieved at 550 °C, since the intensities of some primary peaks enhance and additional diffraction peaks occur. All these diffraction peaks of the sinters at different temperatures can be indexed to zincite ZnO, respectively. With the increase in temperature up to 700 °C, the peaks intensify sharply. It is evident that the diffraction peaks of the samples calcined below 550 °C are broadened, assigned to ZnO nanocrystallites with very small dimensions, and the average crystallite sizes of about 3.5 nm at 450 °C and 5.5 nm at 550 °C, are estimated according to the line width analysis of the diffraction peaks based on the Scherrer formula, respectively.

Fig. 2 shows the micrographs of ESM-templated ZnO prepared at pH 2 and calcined at different temperatures (450 °C, 550 °C, and 700 °C) compared with the original ESM shown in the inset of Fig. 2(a). All the samples have similar microscopic

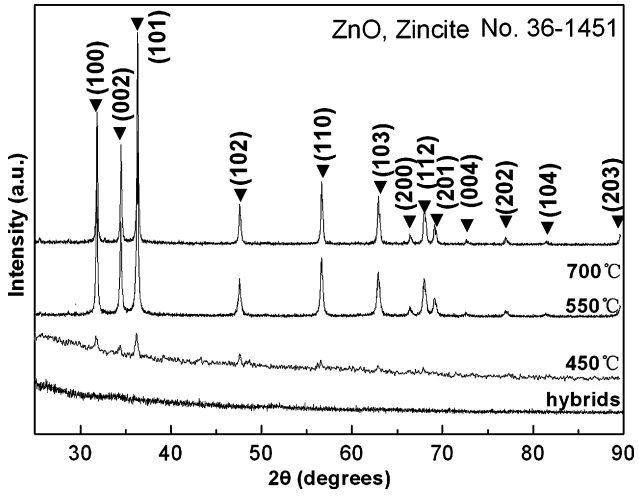

Fig. 1. XRD patterns of the sinters synthesized at various temperatures compared with the templated hybrids (all prepared at pH 2).

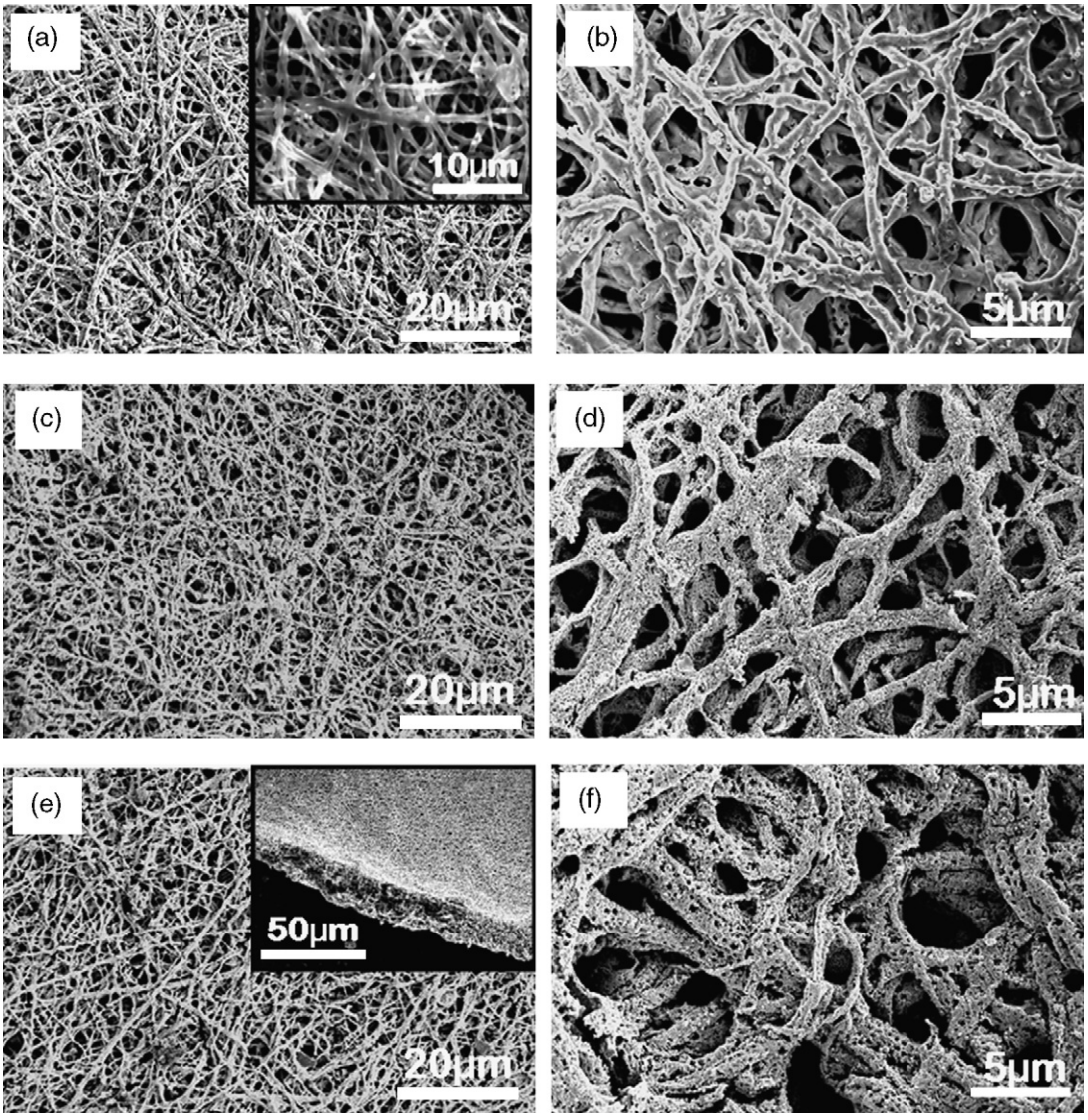

Fig. 2. Typical FESEM images showing interwoven ZnO hierarchy prepared at pH 2 and different temperatures: (a, b) 450 °C, (c, d) 550 °C, and (e, f) 700 °C. The insets in (a) and (e) display the hierarchical interwoven structures of the natural ESM and the cross section of the biomorphic ZnO film at 700 °C, respectively.

features and preserve interwoven and interpenetrated structures of the natural ESM. At higher magnifications, one can see that ZnO fibers range from 0.2 to 1.5 μm in diameter. A careful look at the images also reveals that present ZnO is characterized by repetitious networks consisting of the porous fibers. As ZnO nanocrystallites may grow up with the increase in calcination temperature, the surface of ZnO fiber synthesized below 550 °C looks more glazed in virtue of its smaller nanocrystallite units, which was proved by XRD and TEM results. Above 700 °C, the sample presents a fibrous network composed of interconnected ZnO particles. The inset in Fig. 2(e) shows the cross section of ZnO film prepared at 700 °C, exhibiting the connections of the interwoven fibers. The ZnO film with the thickness of about 25 μm displays hierarchical and subtle structure constructed by cross fibers into interconnected and penetrated meshworks at three dimensions.

Fig. 3 reveals that these ESM-morphic ZnO films synthesized at different temperatures consist of nanocrystallites. As shown in Fig. 3a, ZnO nanocrystallites are found between the two black zones confirmed as the amorphous charring products by EDX results. It indicates that some organic substances are still present at this calcination temperature, which goes in line with the TGA and XRD results. The SAED patterns show that nanoscaled ZnO is of polycrystalline nature, and the diffraction rings are indexed to (100), (101), (102), (110), and (103) diffraction of hexagonal ZnO, although the central spots are not uniform due to the poor crystallization. Fig. 3b displays that ZnO crystallites are about 3.5 nm in diameter and low crystallization. Moreover, some crystallites might be enwrapped by organic macromolecules of ESM remnants. The calcination temperature increased to 550 °C, the better crystallization is accomplished, and the lattice structure can be clearly seen by TEM (Fig. 3c). Considering that each domain having the parallel lattice fringes is a single crystal of ZnO, the average crystallite size is observed to be about 5.5 nm. Notably, the target material at 550 °C is assembled by such small nanocrystallites, which

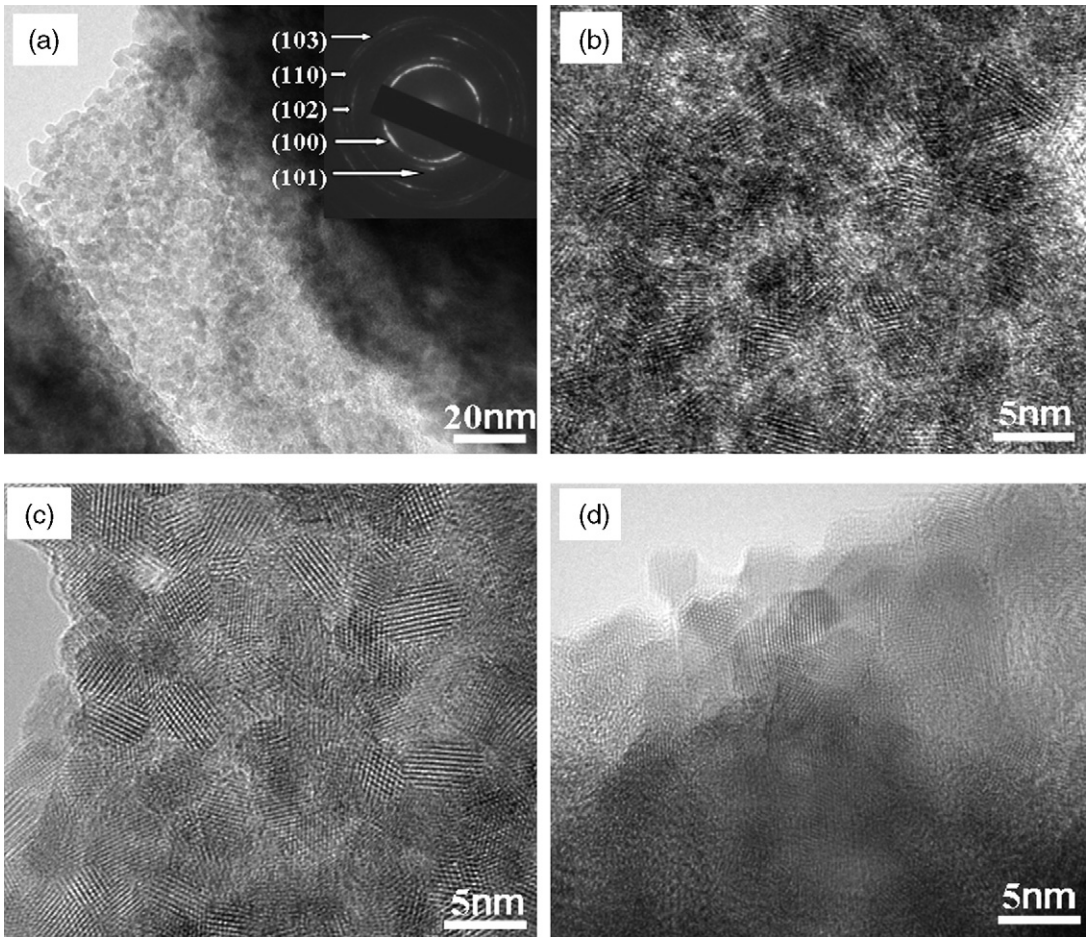

Fig. 3. TEM images of the templated hybrids prepared at pH 2 at various temperatures: (a, b) 450 °C, (c) 550 °C, and (d) 700 °C. The inset in (a) shows corresponding SAED pattern.

probably ascribes to short-chained amino acids of ESM glycoprotein functioned as the capping agents to restrict the growth of zinc oxide nuclei. However, this cage effect is weakened at higher calcination temperature. Fig. 3d shows that at relatively high calcination temperature 700 °C, obtained ZnO nanocrystallites have larger size up to 30 nm. HRTEM and SAED images in Fig. 4 also indicate that the sample at 700 °C has larger crystallite size and exhibits single-crystalline state. The (10–10) planes are imaged of the hexagonal zincite-type crystal with a lattice spacing of 2.86 Å. In addition, the TEM results reveal that the present ZnO synthesized below 550 °C is characterized by the nanoparticle arrays containing some structural defects such as micropores and mesopores. Anyway, accurately defined ZnO nanocrystallites of about 5 nm can be assembled to construct hierarchical films at appropriate calcination temperature 550 °C.

Compared with the above samples prepared at pH 2, present ZnO synthesized at pH 5 and 550 °C exhibits the same interwoven and interpenetrated conformations as shown in Fig. 5. However, one can see that the interwoven fibers are enchased by ZnO sheets. These flakes are inserted perpendicularly along the porous fibers. Thus, a special laminated structure is formed by adjusting the pH value of the impregnant solution, which might engender the template effect on the nucleation and growth of ZnO nanocrystallites. Fig. 6 shows the TEM observations of the above sample. The spot array for the crystal (inset in Fig. 6a) corresponds to the [0001] beam direction. The (0001) face is the large flat face of the ZnO crystal (Fig. 6a). These crystals exhibit flat plate-like morphology and the thickness is

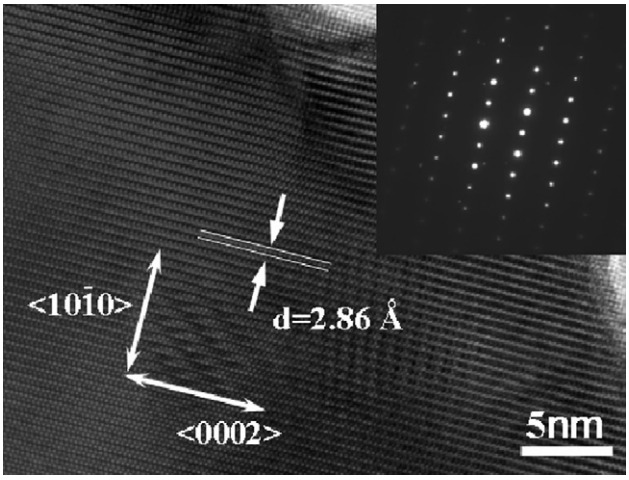

Fig. 4. HRTEM image of biomorphic ZnO prepared at pH 2 and 700 °C. The inset displays corresponding SAED pattern. The imaged lattice spacing amounts to 2.59 Å corresponding to the (002) planes of the zincite structure.

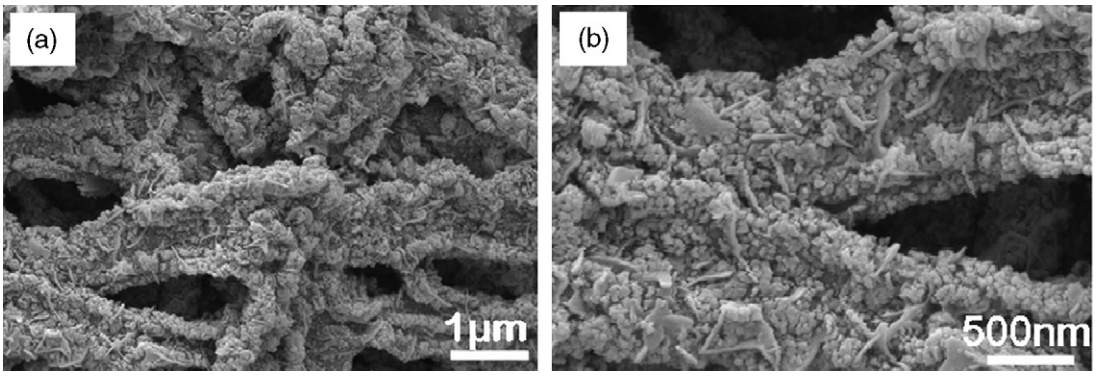

Fig. 5. Typical FESEM images showing (a) the panorama of hierarchical interwoven fibers enchased by hexagonal ZnO sheets prepared at pH 5 and 550 °C; (b) higher magnification of image (a).

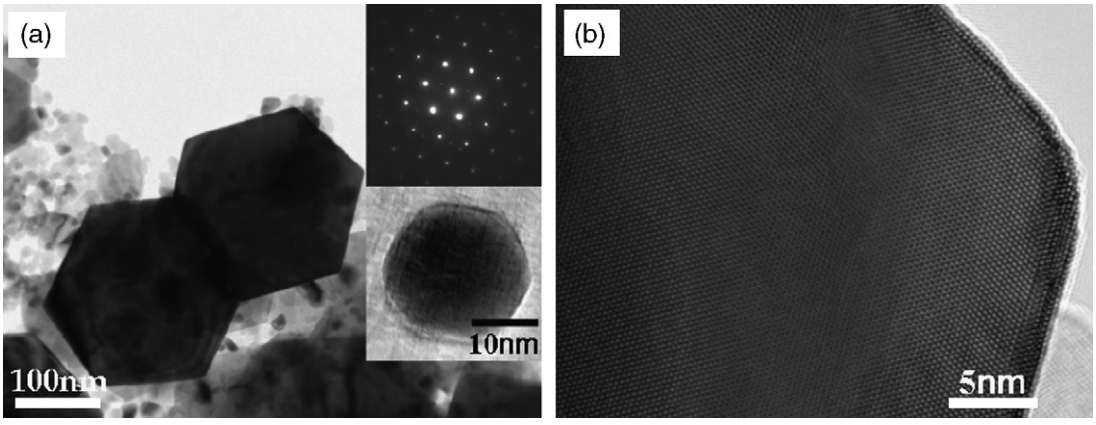

Fig. 6. TEM image of (a) hexagonal ZnO single crystals on interwoven fibers prepared at pH 5 and 550 °C. (b) HRTEM image of corresponds to zincite ZnO. The insets in (a) display corresponding SAED pattern and the primeval nanocrystallite of ZnO single crystal, respectively.

approximately 30–40 nm. Since crystal shapes are dictated by the relative growth rates of the different crystallographic directions, the linking between Zn-precursors and some functional groups from the peptides of ESM glycoprotein may influence the crystal lattice structure of ZnO nuclei and determine the energies of different facets during the nucleation and the growth of zincite-type ZnO. The (0001) face may have lower surface energy and the peptide may bias crystal growth by allowing accumulation of atoms onto the (0001) face. The HRTEM image (Fig. 6b) recorded along [0001] clearly shows the six-fold symmetric lattice image. A detailed analysis of the image indicates no grain boundaries and holes in the crystal structures.

To elucidate the interaction between the Zn-precursors ions and ESM ingredients, and understand ESM multilevel actions during the bioinspired process, FTIR analysis was carried out on original ESM, the templated hybrids and the sinters (Fig. 7a),

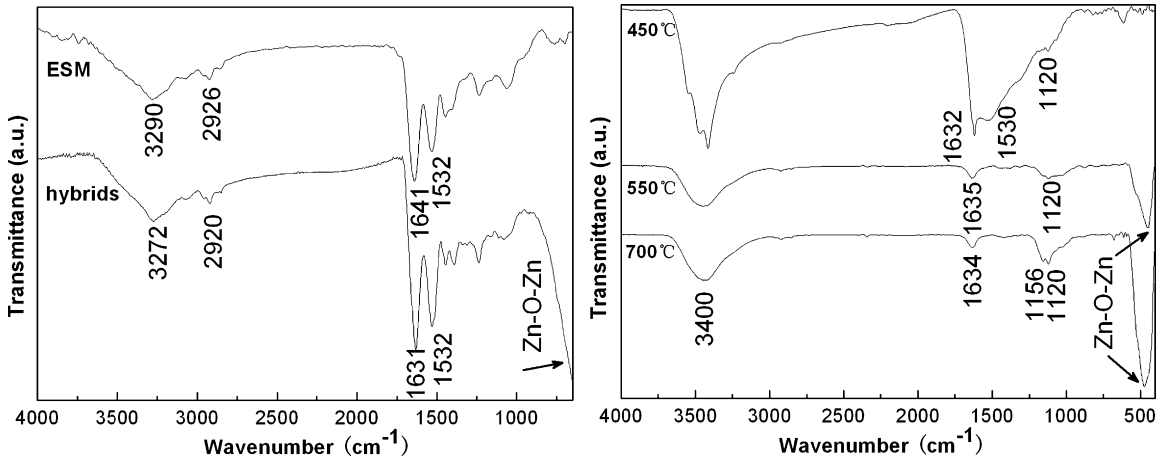

Fig. 7. FTIR spectra of (a) original ESM and templated hybrids and (b) the corresponding sinters at 450 °C, 550 °C, and 700 °C (all prepared at pH 2).

respectively. The spectrum of original ESM shows the diagnostic peaks at 1641, 1532, and 1234 cm^{-1}, which are assigned to the amide I, amide II, and amide III bands of the proteins, respectively. The amide I peak, predominantly corresponding to the C=O stretch, shifts to 1631 cm^{-1} after ESM being immersed in the Zn-precursor solution. This red shift indicates that the C=O bonds in the peptide chains are weakened because of the formation of new chelating bonds between C=O bonds and the zinc ions. It is also detected that the peak corresponded to the vibration band C–H stretching signals of the polypeptides at 3290 cm^{-1} shifts to 3272 cm^{-1}. Such indicate that the inorganic zinc ions are captured on ESM fibers during the soakage. Fig. 7b displays the typical FTIR spectra of the sinters at different temperature. For the sinters at 550 °C and 700 °C, the intense bands appearing at lower frequencies around 480 cm^{-1} are the characteristics of Zn–O–Zn antisymmetric and symmetric vibrations. However, for the sample prepared at 450 °C, such peaks around 480 cm^{-1} cannot be detected, yet a weak peak of C–H at 1530 cm^{-1} appears. Accordingly, it is believed that the sinter at 450 °C contains a mass of amorphous charring remnants enveloping the ZnO nanocrystallites. The bands of the Zn–O–Zn antisymmetric and symmetric vibrations intensify abruptly with the increase in calcination temperature, ascribing to the better crystallization of the sinters ZnO. These analyses go well with the TGA, XRD, and TEM investigations. For all the sinter samples, the peaks at around 3400 cm^{-1} and 1630 cm^{-1} are assigned to the hydroxyl bands of absorbed water. In addition, the peaks appearing in the range between 850 cm^{-1} and 1350 cm^{-1} are assigned to the bending mode of different types of surface hydroxyl groups [30].

By such a bioinspired templating procedure, impregnant ingredients would undergo surface preferred cooperation and interact with bioelements (proteins, polysaccharides, functional residues of ESM ingredients). The interactions are intricate and perplexing. As we known that shell membranes are not mineralized, collagen-based matrix consisted of type I, V, and X collagen being located in the core of each fiber, and surrounded by a soluble glycoprotein mantle [31]. In that way, the glycoprotein macromolecules would act as the soluble species to direct a templating reaction on the ESM fibers during ESM dipped in the $Zn(NO_3)_2$ ethanol solution, further to predefine the nucleation, growth, and assembly of ZnO nanocrystallites into hierarchical nanoarchitectures. The mantle of membrane fibers containing lysozyme is prone to dissociate in the impregnant solution other than the collagenous core. Moreover, lysozyme is one kind of protein with instability under lower acidic medium. Therefore, the morphology of the target material ZnO has an inherent affiliation with the pH value of the impregnant solution. The mantle can exist as a steady overcast at pH < 2.5 while the mantle protein may dissociated extremely at pH 5. Here, lysozyme is partially activated at pH 2 and interacted with the zinc ions as proved by FTIR results. The inorganic Zn-precursors could cross-link and polymerize to form the mesoscopically ordered inorganic/biotemplate complexes due to the self-assembly behavior of the hydrophilic groups of glycoprotein [32]. However, lysozyme is mostly activated under that extreme circumstance with the pH value at 5, leading to the dissociation and disintegration of peptidoglycan-based coating layer. Simultaneously, these peptidoglycan chains may interact with the primeval nuclei of zinc oxide. The (0001) face has lower surface energy and the peptide may bias crystal growth by allowing accumulation of atoms onto the (0001) face. It has also been previously demonstrated that organic binding peptides could control crystal growth and shape [33–35]. The formation of hexagonal ZnO biomorphic films could be ascribed to the surfactant function of ESM biomacromolecules. With the aid of "surfactant molecules", the construction of inorganic hierarchy would be further achieved in the biomolecule–micelle systems. A special templating feature of the current synthesis process is that ordered inorganic structures are replicated from the self-

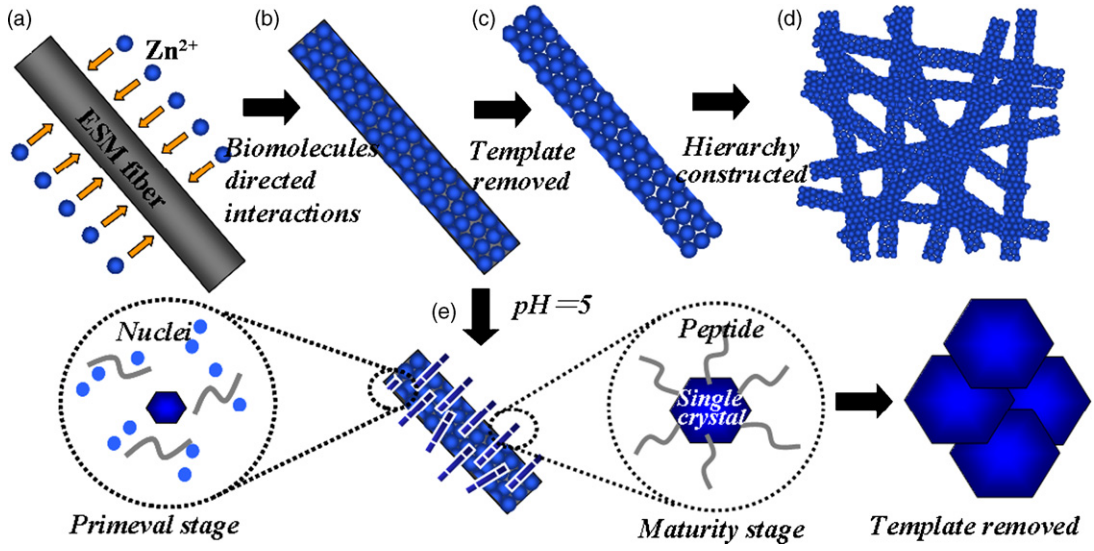

Fig. 8. Schematic illustration of ESM templating process directing the synthesis of hierarchical ZnO: (a) the interactions between the zinc ions and ESM fiber; (b) the assembly directed by ESM biomolecules at pH 2; (c) the formation of porous fibrous ZnO after the remove of ESM; (d) the construction of hierarchical structures; (e) the sheet-enchased fiber prepared at pH 5. Insets in (e) show the primeval stage, maturity stage, and the process after removal of the template, respectively.

Table 1
Synthesis conditions and characters of ESM-templated ZnO materials

Sample	pH[a]	Temperature [b] (°C)	S_{BET}[c] ($m^2\ g^{-1}$)	Pore volume [d] ($ml\ g^{-1}$)	Pore size [e] (nm)
A	2	450	9.86	0.039	28.4
B	2	550	8.92	0.041	18.2
C	2	700	7.58	0.023	35.6

[a] pH value of precursor medium.
[b] Synthesis temperature.
[c] BET surface area calculated from the linear part of the BET plot ($P/P_0 = 0.1$–0.2).
[d] Total pore volume, taken from the volume of N_2 adsorbed at $P/P_0 = 0.995$.
[e] Average pore diameter, estimated using the desorption branch of the isotherm and the Barrett–Joyner–Halenda (BJH) formula.

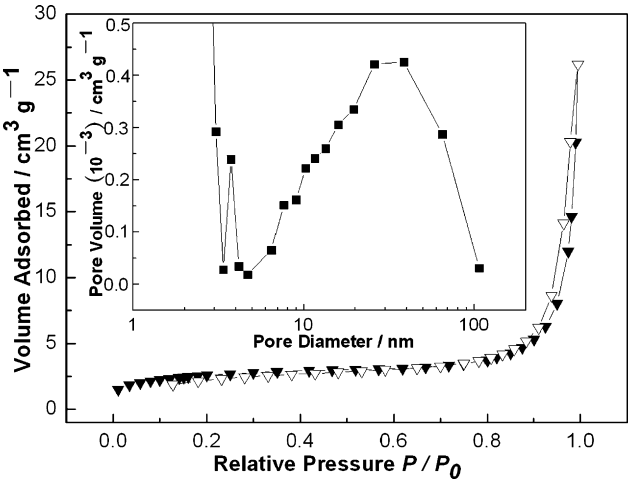

Fig. 9. Nitrogen adsorption–desorption isotherms plots and corresponding pore size distribution plots of ESM-morphic ZnO synthesized at pH 2 and 550 °C.

organized assemblies, and that the biotemplate provides both the chemical revulsant and the physical substrate (Fig. 8).

Nitrogen adsorption–desorption isotherms and corresponding pore-size distributions of ESM-templated ZnO synthesized at different temperatures are listed in Table 1. Typical nitrogen adsorption–desorption isotherm and the corresponding pore-size distribution curve for biomorphic ZnO prepared at pH 2 and 550 °C are shown in Fig. 9. By the Brunauer classification [36], the isotherm of ZnO is characterized as IV-type based on the mesoporous structures. According to the type of isotherm, the sample can be corroborated as mesoporous ZnO with the average pore size 20–30 nm. Additionally, the micropores with the size less than 2 nm are also investigated. Actually, such micropores have been observed in the HRTEM images. Prompted by the porous and hierarchical characteristic, we speculate on that current hierarchical ZnO with a considerable high surface area and narrow pore size distribution is expected to have potential applications in catalysis, solar energy conversion, and optoelectronic devices.

4. Summary

ZnO nanomaterials with hierarchical interwoven conformations have been successfully prepared by a bioinspired templating technique. As-prepared hierarchical ZnO exhibits special porous structures of interconnected fibers assembled by nanocrystallites. The size and the shape of ZnO particles are shown to be also affected by the pH values of the impregnant solution and the calcination temperature. The biotemplate ESM plays crucial roles as a physical substrate and functional macromolecule template to achieve the synthesis. It probably ascribes to short-chained amino acids of ESM glycoprotein functioned as the capping agents for the control on the growth of zinc oxide nuclei. Prompted by its porous character and interwoven meshwork pattern, we suspect that it must be useful in fabricating potential dye-sensitized solar cells providing efficient solar-to-electrical power conversion at low cost. It also makes the hierarchical ZnO nanostructures promising candidates for further applications in field emission microelectronic devices.

Acknowledgements

For the financial support, the authors thank the National Natural Science Foundation of China (grant 10405034), the Major Fundamental Research Project of Shanghai Science and Technology Committee, and the Shanghai Nanotechnology Center (grant 05nm05020). Authors are also thankful to Dr. Yijian Lai for his assistance in the laboratory work.

References

[1] H.D. Yu, Z.P. Zhang, M.Y. Han, X.T. Hao, F.R. Zhu, A general low-temperature route for large-scale fabrication of highly oriented ZnO nanorod/nanotube arrays, J. Am. Chem. Soc. 127 (2005) 2378–2379.
[2] F. Xu, K. Yu, G.D. Li, Q. Li, Z.Q. Zhu, Synthesis and field emission of four kinds of ZnO nanostructures: nanosleeve-fishes, radial nanowire arrays, nanocombs and nanoflowers, Nanotechnology 17 (2006) 2855–2859.
[3] Z.W. Pan, Z.R. Dai, Z.L. Wang, Nanobelts of semiconducting oxides, Science 291 (2001) 1947–1949.
[4] P.X. Gao, Z.L. Wang, Self-assembled nanowire-nanoribbon junction arrays of ZnO, J. Phys. Chem. B 106 (2002) 12653–12658.
[5] J.Y. Lao, J.G. Wen, Z.F. Ren, Hierarchical ZnO nanostructures, Nano Lett. 2 (2002) 1287–1291.
[6] W.J. Li, E.W. Shi, W.Z. Zhong, Z.W. Yin, Growth mechanism and growth habit of oxide crystals, J. Cryst. Growth 203 (1999) 186–196.
[7] H. Wenisch, V. Kirchner, S.K. Hong, Y.F. Chen, H.J. Ko, T. Yao, Evaluation of ZnO substrates for homoepitaxy, J. Cryst. Growth 227 (2001) 944–949.
[8] L. Guo, Y.L. Ji, H.B. Xu, P. Simon, Z.Y. Wu, Regularly shaped, single-crystalline ZnO nanorods with wurtzite structure, J. Am. Chem. Soc. 124 (2002) 14864–14865.
[9] M. Knez, A.M. Bittner, F. Boes, C. Wege, H. Jeske, E. Maiss, K. Kern, Biotemplate synthesis of 3-nm nickel and cobalt nanowires, Nano Lett. 3 (2003) 1079–1082.
[10] R. Seshadri, F.C. Meldrum, Bioskeletons as templates for ordered, macroporous structures, Adv. Mater. 12 (2000) 1149–1151.

[11] W. Zhang, D. Zhang, T.X. Fan, J. Ding, Q.X. Guo, H. Ogawa, Fabrication of ZnO microtubes with adjustable nanopores on the walls by the templating of butterfly wing scales, Nanotechnology 17 (2006) 840–844.
[12] D. Yang, L.M. Qi, J.M. Ma, Eggshell membrane templating of hierarchically ordered macroporous networks composed of TiO_2 tubes, Adv. Mater. 14 (2002) 1543–1547.
[13] Q. Dong, H.L. Su, D. Zhang, In situ depositing silver nanoclusters on silk fibroin fibers supports by a novel biotemplate redox technique at room temperature, J. Phys. Chem. B 109 (2005) 17429–17434.
[14] J.G. Huang, T. Kunitake, Nano-precision replication of natural cellulosic substances by metal oxides, J. Am. Chem. Soc. 125 (2003) 11834–11835.
[15] B.M.W.P.K. Amarasinghe, R.A. Williams, Tea waste as a low cost adsorbent for the removal of Cu and Pb from wastewater, Chem. Eng. J. 132 (2007) 299–309.
[16] S. Weiner, H.D. Wagner, The material bone: structure mechanical function relations, Annu. Rev. Mater. Sci. 28 (1998) 271–298.
[17] S. Kamat, X. Su, R. Ballarini, A.H. Heuer, Structural basis for the fracture toughness of the shell of the conch *Strombus gigas*, Nature 405 (2000) 1036–1040.
[18] S.A. Davis, S.L. Burkett, N.H. Mendelson, S. Mann, Bacterial templating of ordered macrostructures in silica and silica-surfactant mesophases, Nature 385 (1997) 420–423.
[19] J.G. Huang, I. Ichinose, T. Kunitake, Replication of dendrimer monolayer as nanopores in titania ultrathin film, Chem. Commun. (2002) 2070–2071.
[20] H. Yang, N. Coombs, G.A. Ozin, Morphogenesis of shapes and surface patterns in mesoporous silica, Nature 386 (1997) 692–695.
[21] D.Y. Zhao, J.Y. Sun, Q.Z. Li, G.D. Stucky, Morphological control of highly ordered mesoporous silica SBA-15, Chem. Mater. 12 (2000) 275–279.
[22] Z.R.R. Tian, J. Liu, J.A. Voigt, B. McKenzie, H.F. Xu, Hierarchical and self-similar growth of self-assembled crystals, Angew. Chem. Int. Ed. 42 (2003) 414–417.
[23] J.A. Melero, G. Calleja, F. Martınez, R. Molina, M.I. Pariente, Nanocomposite Fe2O3/SBA-15: an efficient and stable catalyst for the catalytic wet peroxidation of phenolic aqueous solutions, Chem. Eng. J. 131 (2007) 245–256.
[24] H.Y. Fan, S. Reed, T. Baer, R. Schunk, G.P. Lopez, C.J. Brinker, Hierarchically structured functional porous silica and composite produced by evaporation-induced self-assembly, Micorporous Mesoporous Mater. 44 (2001) 625–637.
[25] M.P. Pileni, Nanocrystal self-assemblies: fabrication and collective properties, J. Phys. Chem. B 105 (2001) 3358–3371.
[26] S.H. Sun, C.B. Murray, D. Weller, L. Folks, A. Moser, Monodisperse FePt nanoparticles and ferromagnetic FePt nanocrystal superlattices, Science 287 (2000) 1989–1992.
[27] C.B. Murray, C.R. Kagan, M.G. Bawendi, Self-Organization of CdSe nanocrystallites into three-dimensional quantum dot superlattices, Science 270 (1995) 1335–1337.
[28] P.V. Braun, P. Osenar, S.I. Stupp, Semiconducting superlattices templated by molecular assemblies, Nature 380 (1996) 325–328.
[29] J.S. Yin, Z.L. Wang, Ordered self-assembling of tetrahedral oxide nanocrystals, Phys. Rev. Lett. 79 (1997) 2570–2573.
[30] S. Fujihara, T. Maeda, H. Ohgi, E. Hosono, H. Imai, S.H. Kim, Hydrothermal routes to prepare nanocrystalline mesoporous SnO_2 having high thermal stability, Langmuir 20 (2004) 6476–6481.
[31] J.L. Arias, D.J. Fink, S.Q. Xiao, A.H. Heuer, A.I. Caplan, Biomineralization and eggshells: cell-mediated acellular compartments of mineralized extracellular matrix, Int. Rev. Cytol. 145 (1993) 217–250.
[32] P.D. Yang, D.Y. Zhao, D.I. Margolese, B.F. Chmelka, G.D. Stucky, Generalized syntheses of large-pore mesoporous metal oxides with semicrystalline frameworks, Nature 396 (1998) 152–155.
[33] S. Brown, M. Sarikaya, E. Johnson, A genetic analysis of crystal growth, J. Mol. Biol. 299 (2000) 725–735.
[34] J. Aizenberg, G. Lambert, S. Weiner, L. Addadi, Factors involved in the formation of amorphous and crystalline calcium carbonate: a study of an ascidian skeleton, J. Am. Chem. Soc. 124 (2002) 32–39.
[35] Y.P. Kumar, P. King, V.S.R.K. Prasad, Zinc biosorption on *Tectona grandis* L.f. leaves biomass: equilibrium and kinetic studies, Chem. Eng. J. 124 (2006) 63–70.
[36] G.M. Clavier, J.L. Pozzo, H. Bouas-Laurent, C. Liere, C. Roux, C. Sanchez, Organogelators for making porous sol–gel derived silica at two different length scales, J. Mater. Chem. 10 (2000) 1725–1730.